Optical design of a bench-top retinal prosthesis system

By

Paula Choconta

Sc.B., Brown University, 2019

Thesis

Submitted in partial fulfillment of the requirements for the
Degree of Master of Science in Biomedical Engineering at Brown University

PROVIDENCE, RHODE ISLAND

MAY 2020

This thesis by Paula Choconta is accepted in its present form by
the Center of Biomedical Engineering as satisfying the
thesis requirement for the degree of Master of Science.

Date 4/29/2020

Dr. Jonghwan Lee, Advisor

Recommended to the Graduate Council

Date 4/29/2020

Dr. Michael Migliori, Reader

Date 4/29/20

Dr. Kimani Toussaint, Reader

Approved by the Graduate Council

Date 4/29/2020

Marissa Gray

Dr. Marissa Gray, Biomedical Engineering Master's
Program Director

Table of Contents

Abstract

Retinal prostheses stimulate nerve cells at different target locations along the visual pathway treat vision loss. Electrode-based retinal prosthesis implants have been used to restore vision in subjects with vision loss. These implants have shown favorable results, but there are limitations, such as limited resolution and reduced functionality over time. To bypass the limitations of electrode-based implants, a contact-free and spatially selective stimulation method such as optical stimulation of nerve cells can be used. Near-infrared light can be used to activate neuron cells by inducing a temperature change in target cells without tissue damage. This paper focuses on the NIR stimulation of retinal ganglion cells to optimize optical parameters for a bench-top retinal prosthesis system and examines the feasibility of non-invasive retinal prosthesis through the numerical simulation of laser projection on the retina.

Introduction

According to the World Health Organization there are an estimated 285 million people visually impaired globally, 39 million of which are blind.[1] Various diseases cause blindness, the most common of which are cataracts and glaucoma. Degeneration of the retina caused by diseases such as age-related macular degeneration and retinitis pigmentosa also contribute to blindness and have limited ways to prevent or halt the progression of visual impairment.[2] Loss of retinal photoreceptors and/or retinal pigment epithelium while the inner retina remains intact is characteristic of these outer retinal diseases.[3] Age-related macular degeneration is associated with the progressive loss of photoreceptors, and thus vision, in ageing populations.[4] Retinitis pigmentosa is a hereditary retinal degeneration disease characterized by the loss of photoreceptors.[5] Since the retinal ganglion cells are preserved in outer retinal diseases, retinal prosthetic devices prove to be key interventions to restoring some functional vision.

Background

Currently, there are a few methods for treating vision loss due to retinal degeneration, such as photodynamic and conventional laser therapy. Innovative approaches such as retinal transplantation and gene therapy have proven useful for reducing or reversing vision loss. In cases where retinal ganglion cells are preserved, retinal prosthesis may prove to be effective interventions. The application of electrical stimulation of different locations of the visual pathway, including the visual cortex, the optic nerve, and the retina has proven to cause subjects to perceive an artificial visual percept, or phosphene. Changing the target area of the electrical stimulation on the cortex changed the spatial psychological location of the phosphene. The stimulation excites the target neurons by opening voltage-gated ion channels, bypassing the chemically gated channels in the target cells. Once a certain potential is reached within the target neuron, an action potential is triggered through an all-or-none mechanism. The action potential then triggers a cascade of signals that pass through the visual pathway to mimic light stimulation.[2] Thus, stimulation of the visual pathway leads to light perception.

Rudimentary light perception can be achieved through electrical, magnetic, mechanical, thermal, chemical and optical stimulation of the visual pathway.[6] Electrical stimulation is considered the gold standard for retinal prosthesis; however, there are numerous limitations. Electrical stimulation requires the implantation of an electrode array that applies the electrical signal, which intrinsically damages the tissue when implanted. Additionally, even after successful implantation, there is a 40% drop in the number of functional electrodes within the first 18 months after implantation, which prevents the chronically implanted electrode from functioning sufficiently over time.[7] Implants designed with favorable visual field and resolution may work well in theory, but fail to perform as expected in trials due to high failure of electrodes. Electrical stimulation also lacks spatial specificity as the electric currents spread in

the conductive media of the retina, preventing the excitation of single cells. Existing electrical retinal prosthesis have a resolution of around 150 μm, while retinal ganglion cells are approximately 10 μm in diameter, meaning that multiple neurons are activated per stimulus.[8] The only commercially available retinal implant, the Argus II, restores a visual field of approximately 11 to 19 degrees,[9] which is marginal when compare to a normal human visual field of 135 degrees side to side and 160 degrees up and down.[10] Electrode-array based retinal prosthetics restore some functional vision in patients, but the restored vision has a visual acuity of 20/1200, which would still classify subjects as legally blind, as defined by a visual acuity of 20/200.

Due to the implantation-associated limitations of electrical stimulation, non-implantation methods for remote activation of retinal neurons are being pursued. One such technology is optogenetics, where light-responsive genes are delivered into target tissue regions in order to excite or inhibit neural activity through the modulation of a specific wavelength of light. While optogenetic technologies are promising for clinical applications since they offer excellent temporal and spatial resolution, there are concerns of genetic manipulation of humans.[11]

Over a decade ago, researchers established a "contact-free, damage-free, spatially selective, artifact-free method" of neural stimulation where a pulsed infrared laser was used to stimulate peripheral nerves. Radiant exposure was kept below the damage threshold and resulted in compound nerve action potentials and compound muscle action potentials. When compared to action potentials caused by electrical stimulation, there was no difference in conduction velocities, indicating that the action potentials are the same regardless of the mechanism of stimulation.[6] Infrared stimulation is an effective alternative to electrical stimulation since it produces remote activation at high spatial resolution as the pulsed infrared laser energy can be delivered to the target site through an optical fiber without the need for direct contact. Pulsed

infrared laser energy is absorbed by water to produce a localized increase in temperature. This temporary increase in temperature within the target tissue has been proposed to cause an increase in membrane capacitance, which depolarizes the cell and initiates an action potential.[12] It has also been discovered that infrared laser irradiation activates TRPV4 (transient receptor potential cation channel subfamily V, 4) channels, which display temperature sensitivity and are the most common type of TRPV channels in retinal ganglion cells. It can be assumed that any TRPV channel can be activated by pulsed infrared laser energy as long as a sufficient thermal change is reached to alter the membrane voltage.[13]

Both proposed mechanisms involve the bulk heating of tissue through the absorption of energy by water. Stimulation by wavelengths between 1,400 to 2,200 nm is required for energy absorption by water to elevate the temperature. However, bulk heating can cause tissue damage and should be avoided in clinical applications. Additionally, wavelengths in the required range to be absorbed by water have limited penetration depth in tissue, and thus limited application.[14]

To bypass the limitations of pulsed infrared stimulation, near infrared (NIR) light can be used instead. Light between 700-900 nm penetrates tissue deeper than infrared light or visible light and induces less bulk heating in the tissue due to a lower absorption coefficient in water. In fact, NIR light exhibits negligible water absorption, and thus, NIR stimulation requires the use of gold nanorods (AuNRs) for localized heating. The AuNRs absorb energy from NIR light for heat generation through localized surface plasmon resonance that converts photons into heat. By altering the size and aspect ratio of the AuNRs, they can be modified for use with specific wavelengths. AuNRs are widely used in different applications, so there is a good understanding in how to deliver the AuNRs to target sites, making them ideal for use in NIR stimulation, although the toxicity of gold nanoparticles injected into the retina in the long term requires

further investigation.[15] AuNR-enhanced NIR stimulation is a contact free and spatially selective method for remotely activating ganglion cells to induce vision and its theoretical performance should be compared to existing methods to investigate the feasibility of non-invasive retinal prosthesis.

Bench-top NIR Stimulation of Retinal Ganglion Cells

AuNR-enhanced NIR stimulation of retinal ganglion cells can be used to induce visual perception in blind subjects. By rapidly scanning the laser beam across a target area on the retina, multiple neurons can be excited to create visual stimuli representing a scene as captured by an external camera. This bench-top retinal prosthesis system will function as a proof of concept of AuNR-enhanced NIR stimulation of retinal ganglion cells with single-cell resolution to successfully produce visual percepts in subjects. A bench-top retinal prosthesis system consists of an ergonomic chest rest that guides the subject's head into place to align the position of the eye and secures the position. A probing laser ($\lambda = 785\ nm$) is mounted within the system along with a galvo mirror. The movement of the galvo mirror dictates the laser beam scanning along the retina. The probing laser beam is then pulsed and scanned along the retina to stimulate retinal ganglion cells and promote visual percepts in the subject. For an optimal retinal prosthesis system, the possible visual field and visual field resolution should be maximized. Prior to the instrumentation of a bench-top system, parameters such as the appropriate galvo mirror specifications and laser beam diameter size need to be established to optimize visual field for the system.

Optical Set-Up and Input Parameters

In the proposed set-up, a collimated NIR laser is directed at a galvo mirror, which redirects the laser beam to the eye. One of the most important parameters of the system is the distance between the galvo mirror and the surface of the lens or the patient eye. Commercially available retinal OCT systems have a working distance ranging from 2.5 cm to 8 cm.[16] Through the modulation of the galvo mirror angle, the laser beam can be directed at different positions onto the back of the eye.

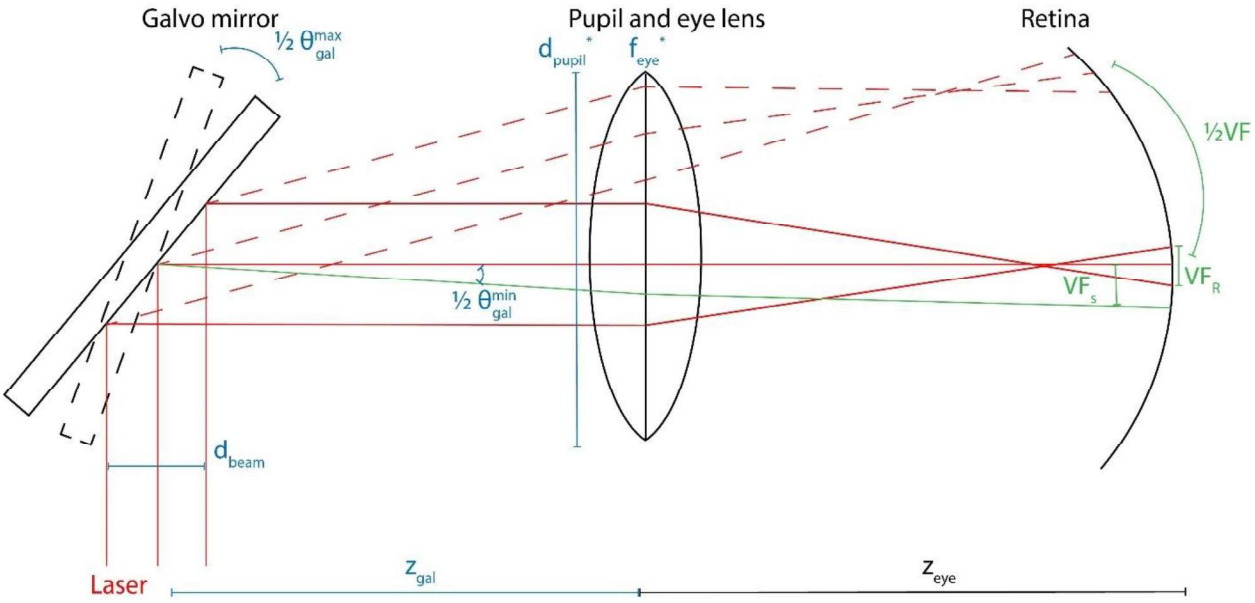

*Figure 1. Proposed optical set-up for AuNR-enhanced NIR stimulation of retinal ganglion cells. Blue represents the input parameters of the system; green represents the desired output parameters. * indicates that the parameters are uncontrollable human factors. VF = visual field.*

The possible scanning angle of the laser beam depends on the scan angle of the chosen galvo mirror and will affect the resulting visual field. If the scan angle is sufficiently large such that the galvo mirror allows the laser to scan an area larger than the pupil, then the effective maximum angle of the laser scan on the retina is determined by the pupil diameter and galvo position. Otherwise, the maximum scan angle is defined by the galvo mirror maximum angle.

$$\theta_{eff}^{max} = min(2tan^{-1}(\frac{d_{pupil}}{z_{gal}}), \theta_{gal}^{max}) \quad \text{(Eq. 1)}$$

The minimum angle scan angle of the galvo mirror determines the visual field step since it establishes the distance the laser beam can move per step (per unit time), and thus, step size on the retina and of the visual field. The minimum angle describes the galvo mirror's inherent precision and depends on multiple factors, such as the galvo mirror specifications, scanning strategy, and voltage noise. For the present study, a precision in the order of 1% was assumed.

Another important input parameter of the system is the size of the laser beam. The laser beam diameter heavily influences the diffraction-limited beam spot size projected onto the retina,

which may determine the visual field resolution. In this system, the laser beam diameter is determined by the chosen laser and can be modulated by an optical collimator to create a laser beam of the desired size. We used the typical range for laser beam diameter, 1 to 10 mm.

Table 1. Input parameters.

Variable	Symbol	Range	Unit	Note	Reference
Distance between the galvo mirror and the eye surface	z_{gal}	2.5 to 10	cm	Estimated range from commercially available retinal OCT systems	Qing et al.
Laser beam diameter at galvo mirror	d_{beam}	1 to 10	mm	Beam size controlled by a collimator	
Focal length of the eye	f_{eye}	22 to 25	mm	The minimum calculated using Eq. 2	
Pupil diameter	d_{pupil}	2 to 8	mm		Walker et al.
Maximum scan angle of the galvo mirror	θ_{gal}^{max}	10 to 40	deg	Determined by galvo mirror specifications, position and pupil size	
Minimum scan angle of the galvo mirror	θ_{gal}^{min}	0.1 to 0.5	deg	Estimated with a precision in the order of 1%	

Two uncontrollable human characteristics of the eye, pupil size and the focal length of the eye, also may affect the visual field of the system. The pupil size varies patient by patient and cannot be controlled. Emmetropic pupil size in adults ranges from 2 to 4 mm in diameter in bright light and 4 to 8 mm in the dark.[17] The focal length of the eye depends on the distance of the object being focused on. When a normal subject is focusing on an object infinitely far away, the focal point falls onto the retina and the focal length is approximately the size of the eye. The average size of a human eye, or distance between eye lens and the retina, is 25 mm.[18] This determines the upper limit of the focal length. When the subject is focusing on a close object, the focal point falls short of the retina and the focal length is smaller than the size of the eye. This

lower limit can be determined using the thin lens equation for an object at the closest distance within the range of normal vision (b = 20 cm for Eq. 2), which turned out to be 22 mm.

$$\frac{1}{f_{eye}} = \frac{1}{z_{eye}} + \frac{1}{b} \qquad \text{(Eq. 2)}$$

Calculations

We investigate how the visual field and its resolution of the system depends on all six input parameters: distance between the galvo mirror and the eye, laser beam diameter, focal length of the eye, pupil size, maximum scan angle and minimum scan angle. The visual field outcome of the system can be simulated by tracing the chief laser ray from the galvo mirror through the pupil to the eye using ray transfer matrix (RTM) analysis. RTM analysis describes a light ray by a 2x1 vector and an optical element by a 2x2 matrix. Using RTM analysis, incoming ray, defined by its incident angle to the plane of the optical element and distance from the optical axis, can be traced through the system and the resulting output ray can be calculated. Given a 2x1 vector consisting of the x distance from the optical axis and the angle of incident θ, the output angle and distance from the optical axis can be found.

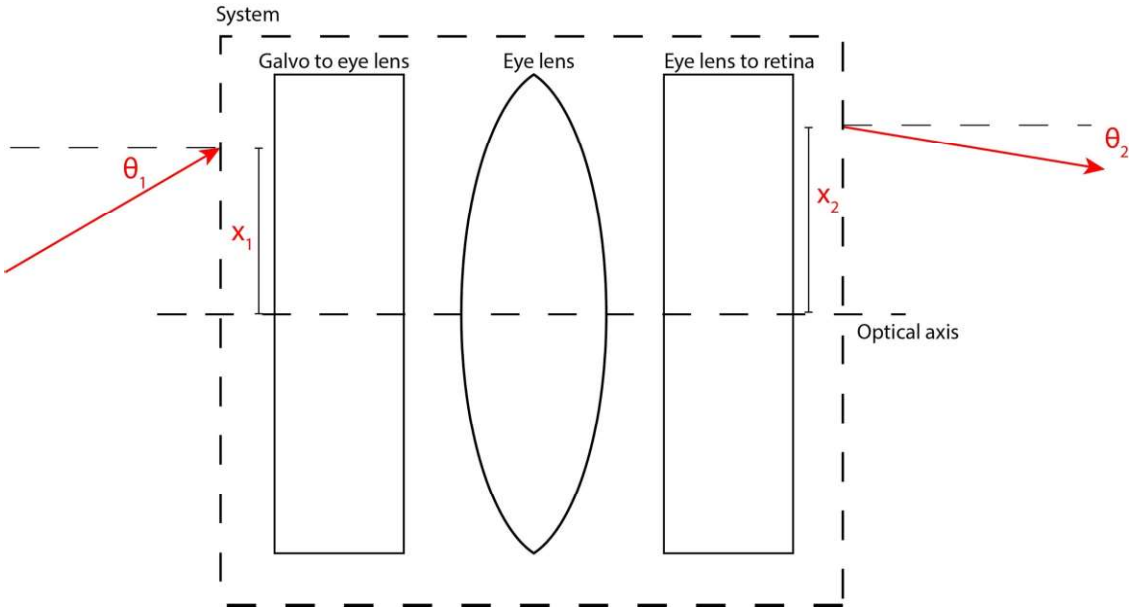

Figure 2. Ray transfer matrix analysis of the system. Any incoming ray, described by its incident angle θ_1 and distance from the optical axis x_1, can be traced through the system to an output ray with incident angle θ_2 and distance x_2. The RTM of the system consists of the RTM of each optical element multiplied together.

If a beam propagates through several optical elements, including any air spaces between them, a single matrix for the entire system can be found as the matrix product of all elements. The model proposed here consists of three elements: the free space from the galvo mirror to the

eye, the eye lens (approximated as a thin lens), and the free space from the eye lens to the retina. The RTM of the system is defined by multiplying the RTM of each element.

$$RTM_{gal,eye} = \begin{bmatrix} 1 & z_{gal} \\ 0 & 1 \end{bmatrix} \quad \text{(Eq. 3)}$$

$$RTM_{eye\ lens} = \begin{bmatrix} 1 & 0 \\ -\frac{1}{f_{eye}} & 1 \end{bmatrix} \quad \text{(Eq. 4)}$$

$$RTM_{eye\ lens,retina} = \begin{bmatrix} 1 & z_{eye} \\ 0 & 1 \end{bmatrix} \quad \text{(Eq. 5)}$$

$$RTM_{system} = RTM_{eye\ lens,retina} \cdot RTM_{eye\ lens} \cdot RTM_{gal,eye} \quad \text{(Eq. 6)}$$

Using an input ray $p_{max\ angle}^{input}$with an angle equal to the maximum scanning angle a_{gal}^{max} and incident at the optical axis, an output ray corresponding to the distance that is covered on the retina.

$$p_{max\ angle}^{input} = \begin{bmatrix} 0 \\ \frac{1}{2}\theta_{eff}^{max} \end{bmatrix} \quad \text{(Eq. 7)}$$

$$p_{max\ angle}^{output} = \begin{bmatrix} x_{max} \\ \theta_{max\ angle}^{output} \end{bmatrix} = RTM_{system} \cdot p_{max\ angle}^{input} \quad \text{(Eq. 8)}$$

From the output ray, the visual field of the system can be calculated using a conversion factor. According to literature, one degree of visual angle equals 288 μm on the retina, without correction for shrinkage.[19] Thus, the degrees of visual field can be found from the $x$distance of the output ray (the first element of $p_{max\ angle}^{output}$, x_{max}) using the conversion factor of $\alpha = \frac{1^\circ}{288\ \mu m}$. Note that we used the half of the maximum angle in Eq. 7 for RTM analysis and thus need to multiply 2 in Eq. 9 for the full visual field. We use the effective maximum angle, not simply the maximum scan angle of the galvo mirror since pupil diameter will limit the arc that can be scanned. A large maximum scan angle is limited by the size of the pupil since any distance

scanned outside of the pupil is not of interest in this system. Thus, the size of the of the pupil limits the maximum scan angle of the system.

$$VF = 2\, x_{max} \cdot \alpha \quad \text{(Eq. 9)}$$

The corresponding visual field step size of the laser on the retina is found using the minimum scanning angle a_{gal}^{min} as the incident angle and an input ray $p_{min\ angle}^{input}$.

$$p_{min\ angle}^{input} = \begin{bmatrix} 0 \\ \theta_{gal}^{min} \end{bmatrix} \quad \text{(Eq. 10)}$$

$$p_{min\ angle}^{output} = \begin{bmatrix} x_{min} \\ \theta_{min\ angle}^{output} \end{bmatrix} = RTM_{system} \cdot p_{min\ angle}^{input} \quad \text{(Eq. 11)}$$

Using the same method as used for visual field, the visual field step can be derived from the first element x_{min} of the output ray $p_{min\ angle}^{output}$.

$$VF_s = x_{min} \cdot \alpha \quad \text{(Eq. 12)}$$

When the laser beam is collimated onto the retina, it may not necessarily be exactly focused on the retina due to the uncontrollable nature of human eye focus. As illustrated in Figure 1, the chief and peripheral rays of the laser beam may meet before they fall on the retina. Thus, the focal point would be before the retina. In an unfocused case like this, the beam spot size is determined by the divergence of the chief and peripheral rays. When the laser beam is targeted at the center of the pupil and parallel to the optical axis, the x distance of the incoming ray is given by the beam size of the laser and the incident angle $\theta = 0$. If the diameter of the beam as it is incident on the pupil is smaller than the size of the pupil, then the $x$distance is defined by the diameter of the laser beam. However, if the diameter of the beam is larger than the size of the pupil, then the x distance is limited by the size of the pupil.

$$p_r^{input} = \begin{bmatrix} min(\frac{d_{beam}}{2}, \frac{d_{pupil}}{2}) \\ 0 \end{bmatrix} \quad \text{(Eq. 13)}$$

Thus, Eq. 13 corresponds to an unfocused case and the corresponding visual field resolution can be determined using ray transfer matrix analysis to analyze the divergence between the chief and peripheral rays. The visual field resolution is twice the size of the divergence between the chief and peripheral rays.

$$p_r^{output} = \begin{bmatrix} x_r \\ \theta_r^{output} \end{bmatrix} = RTM_{system} \cdot p_r^{input} \quad \text{(Eq. 14)}$$

$$VF_r^{unfocused} = 2x_r \cdot \alpha \quad \text{(Eq. 15)}$$

If the chief and peripheral rays meet at the retina, then the beam size on the retina is determined by the diffraction limited spot size. For this focused case, we calculated the spot size to be the full width half maximum (FWHM) size of the Airy disk of the laser beam. Although the laser beam is better modeled by a Gaussian beam, we assumed a plane wave here to be consistent with the above RTM analysis. When the Gaussian beam model is used, we should use a Gaussian RTM analysis, detail of which will be briefly discussed in the Discussion section. The Airy disk size of a plane light wave is determined by the wavelength and the numerical aperture (NA) of the system. The NA of the system is defined by the refractive index of the eye, the radius of the pupil r_{pupil} and the focal length of the eye. In an unfocused case, the beam spot size is dictated by the wavelength of the laser beam.

$$NA = n_{eye} \frac{r_{pupil}}{\sqrt{{f_{eye}}^2 + {r_{pupil}}^2}} \quad \text{(Eq. 16)}$$

$$FWHM_{airy} = 0.42 d_{airy} = .51 \frac{\lambda}{NA} \quad \text{(Eq. 17)}$$

$$VF_r^{focused} = FWHM_{airy} \cdot \alpha \quad \text{(Eq. 18)}$$

The effective visual field resolution is given by the maximum between the unfocused and focused cases.

$$VF_r^{eff} = max(VF_r^{unfocused}, VF_r^{focused}) \quad \text{(Eq. 18)}$$

Results

The visual field, visual field step, and visual field resolution were calculated for all combinations of input parameters listed in Table 1. This results section presents how those three outputs depend on six input parameters: distance between the galvo mirror and the eye, laser beam diameter, focal length of the eye, pupil size, maximum scan angle and minimum scan angle. A multiple linear regression analysis of the resultant visual field revealed that neither the size of the laser beam nor the minimum scan angle influences the visual field of the system. This is expected, as the visual field depends on the maximum arc that can be scanned, which is determined mostly by the distance between the galvo mirror and the eye and the maximum scanning angle of the galvo mirror, as well the focal length of the eye and pupil size, which are inherent characteristics of the human eye. This can be verified by calculating the standard deviation of the visual field across all values of the laser beam size and the minimum scan angle. The standard deviation for both of these was found to be essentially zero, confirming that both input parameters have a negligible effect on the visual field. Thus, the visual field turned out to depend on four parameters: distance between the galvo mirror and the eye, focal length of the eye, pupil size, and maximum scan angle.

Table 2. Linear regression analysis of visual field.

Variable	Coefficient	p-value
z_{gal}	-140.86	0
d_{beam}	1.7427e-12	1
f_{eye}	780.57	0
d_{pupil}	1342.5	0
θ_{eff}^{max}	0.86801	2.109e-80
θ_{gal}^{min}	2.7571e-12	1

The visual field outcome was found to be distributed between 0 and 28 degrees. Normally, the human monocular visual field extends approximately 60 degrees upward, 75 degrees downward, 100 degrees laterally and 60 degrees medically.[10] To find out what factors resulted in large visual fields (larger than 20 deg), the visual field for all four input parameters was plotted.

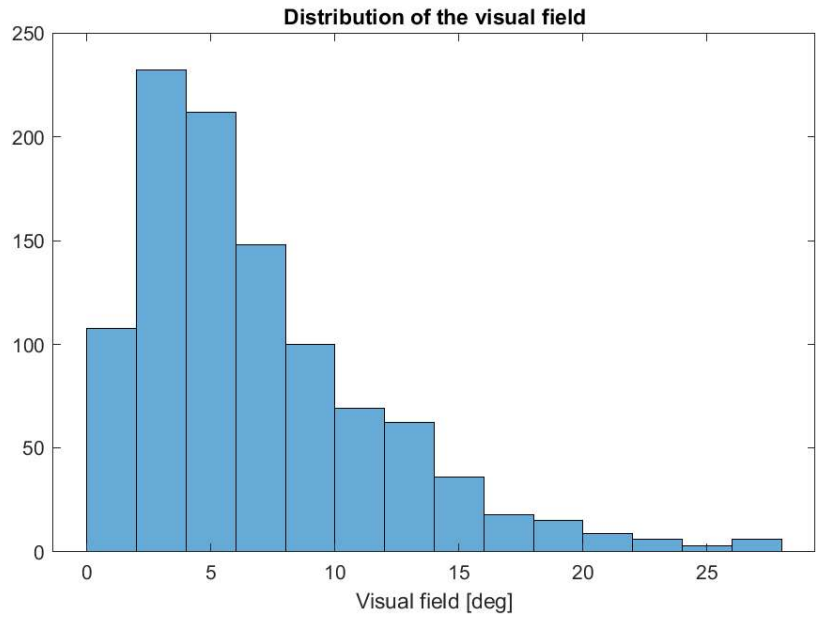

Figure 3. Histogram of the visual field outcome.

Figure 4 reveals that the focal length of the eye affects the visual field minimally compared to the other parameters. The focal length of the eye plays a large role in determining the spot size, and the minimal effect on the overall visual field is expected. The maximum scan angle of the galvo mirror also appears to minimally affect the resultant visual field. There seems to be little difference between different maximum scan angles except in cases where the maximum angle was 10 deg and the pupil size was large (6 and 8 mm). This may be because in most cases, the limiting factor for the maximum scan angle is the pupil size. A closer look at the distribution of the visual field for each maximum scan angle indicates that the median visual field for all maximum scan angles are about the same, suggesting that the negligible differences may indeed be due to the limitation set by the pupil size. A one-way ANOVA test confirmed that

10 degrees was the only group that varied significantly. This indicates that the system does not require a maximum scan angle greater than 20 degrees as pupil diameter limits its effect on visual field.

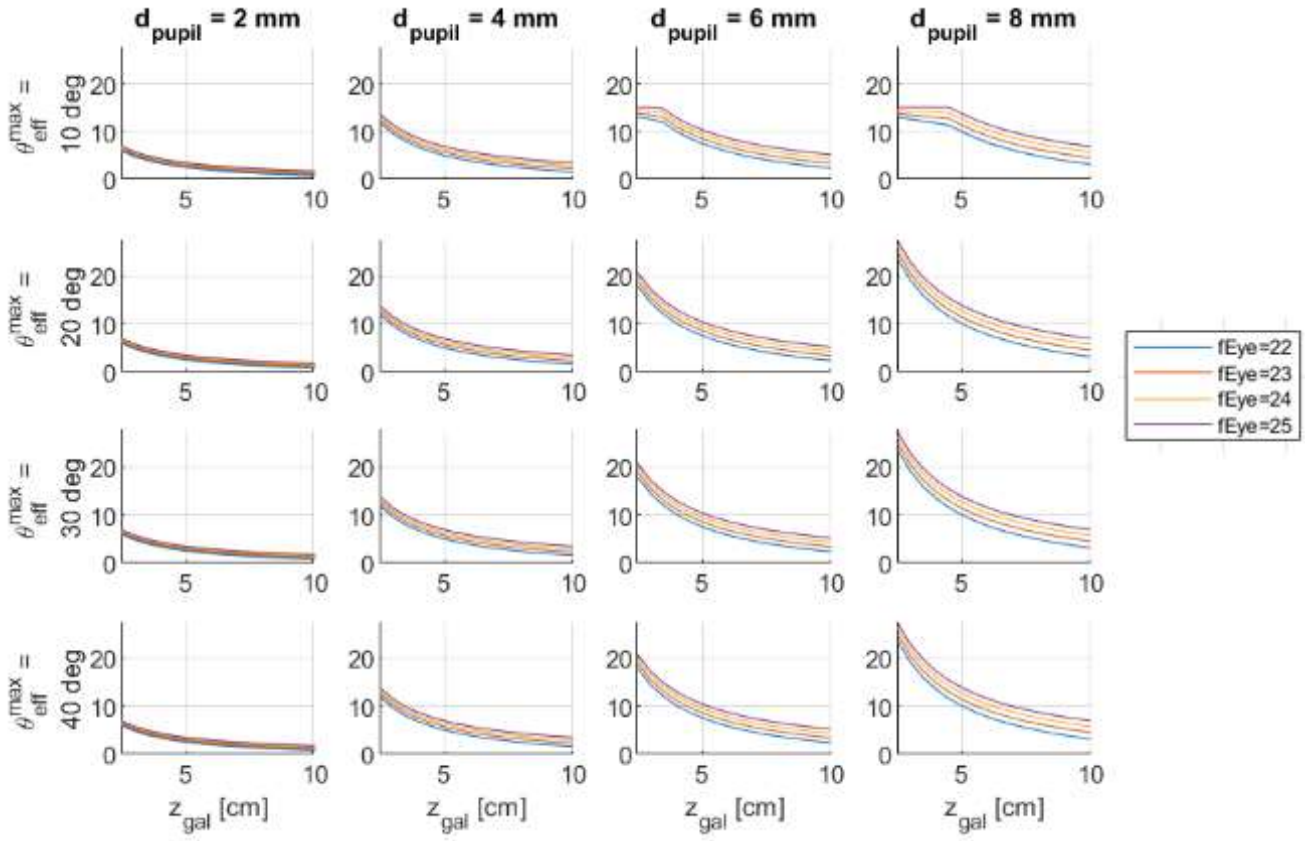

Figure 4. Resultant visual field for the all combinations of the four input parameters.

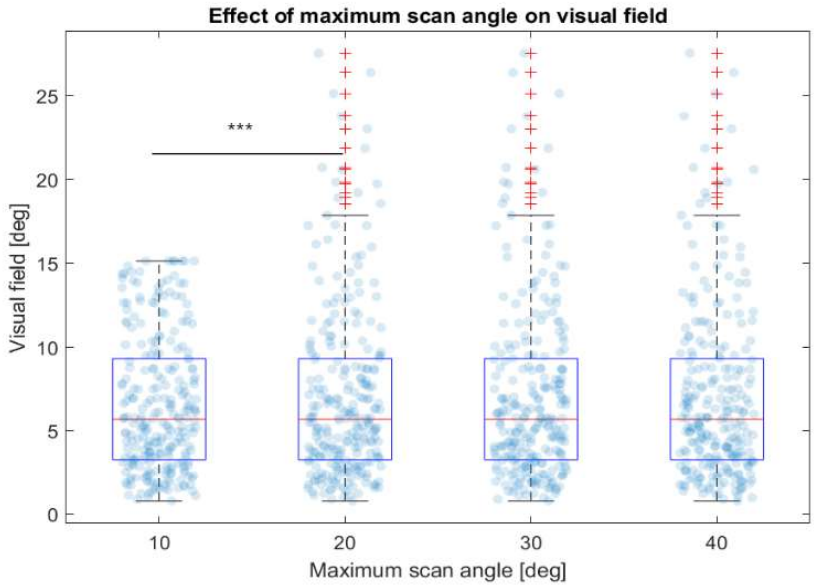

Figure 5. Effect of the maximum scan angle of the galvo mirror on the visual field. A one-way ANOVA test indicated 10 degrees as the only statistically different group.

The largest factor on the visual field that can be controlled in the system is the distance between the galvo mirror and eye. The closer the galvo mirror is to the eye, the larger the resultant visual field. A one-way ANOVA analysis of the effect of the distance between galvo mirror and eye on visual field reveals that after 8.5 cm, the effect on visual field is no longer statistically significant. This suggest that the operational range of the distance can be limited between 2.5 and 8.5 cm, which aligns closely to the working distance of commercially available retinal OCT systems.

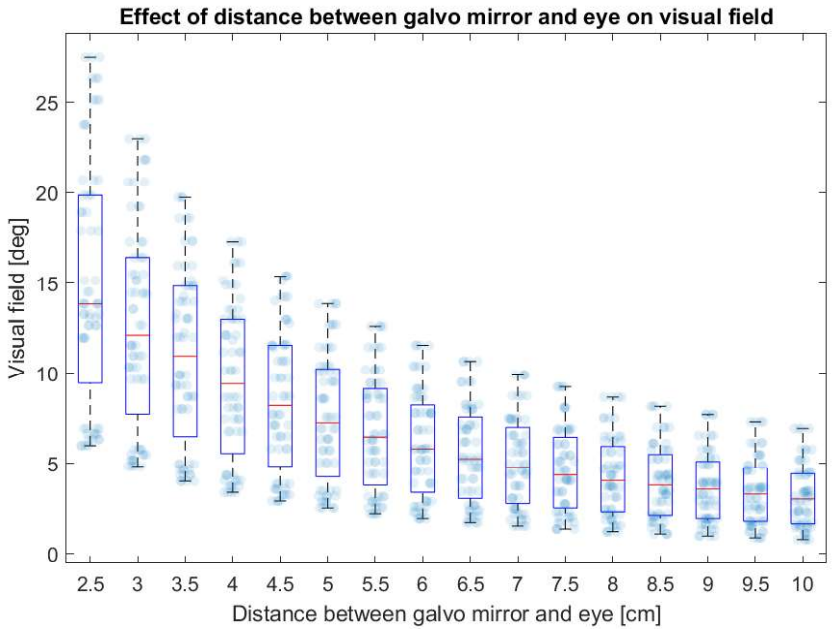

Figure 6. Effect of the distance between the galvo mirror and eye on the visual field.

The linear regression analysis suggests that pupil size is the largest influencer on the visual field. This is supported by investigating the distribution of the visual field according to pupil size. The median visual field varied between pupil sizes and the larger the pupil, the larger the resultant visual field. While pupil size greatly influences the visual field, it is not a controllable parameter in the given system, just as the focal length of the eye is not controllable. As both factors are not controllable in practice, we should predict how the visual field would be affected by those factors. For a given maximum scan angle (20 deg) and distance between the galvo mirror and eye (5 cm), the visual field increases with an increased focal length of the eye. Visual field also increases with pupil size. The largest possible visual field in this configuration was 13.86 degrees when the focal length is 25 mm and the pupil size is 8 mm. The largest possible visual field across all tested configurations was 27.54 degrees when the maximum scan angle is greater than 20 degrees, the distance was 2.5 cm, the focal length was 25 mm, and the pupil size was 8 mm.

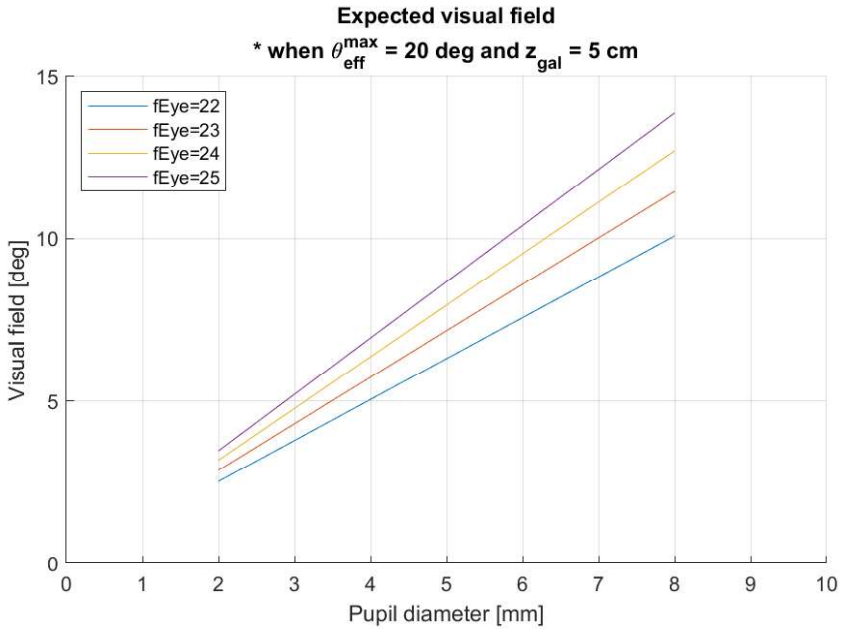

Figure 7. Effect of uncontrollable human eye factors on the visual field.

A linear regression analysis of the visual field step indicates that the laser beam size, pupil size and maximum scan angle do not influence the visual field step.

Table 3. Linear regression analysis of visual field step.

Variable	Coefficient	p-value
z_{gal}	-1.2044	0
d_{beam}	9.284e-14	1
f_{eye}	51.63	0
d_{pupil}	1.8511e-13	1
θ_{eff}^{max}	1.6967e-14	1
θ_{gal}^{min}	72.429	0

This was double-checked with the standard deviation across these parameters, which was found to be zero for all three. Thus, only the distance between the galvo mirror and eye, focal

length of the eye, and the minimum scan angle affect the visual field step. Among these, the minimum scan angle and focal length of the eye affected the visual field step the most.

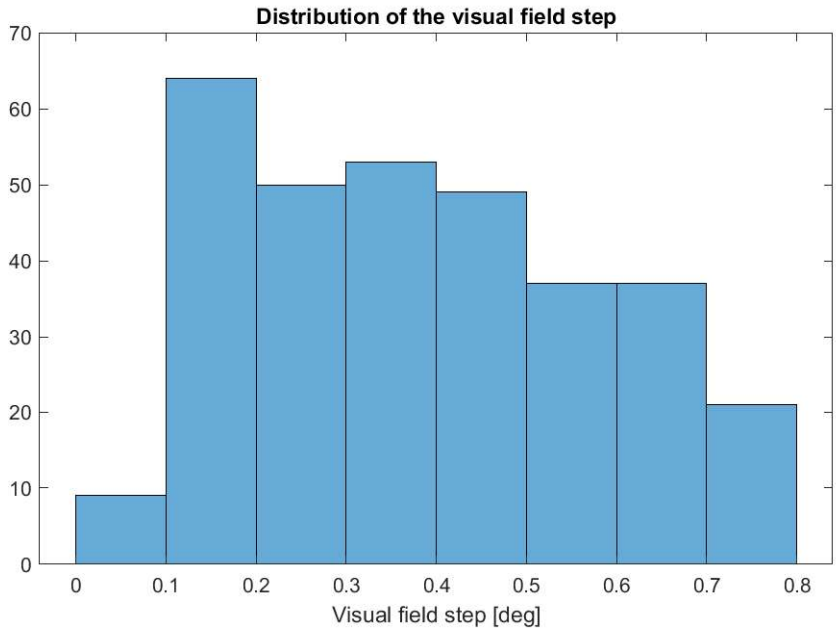

Figure 8. Histogram of the resultant visual field step.

The visual field step outcome for the system is distributed between 0.07 and 0.8 degrees.

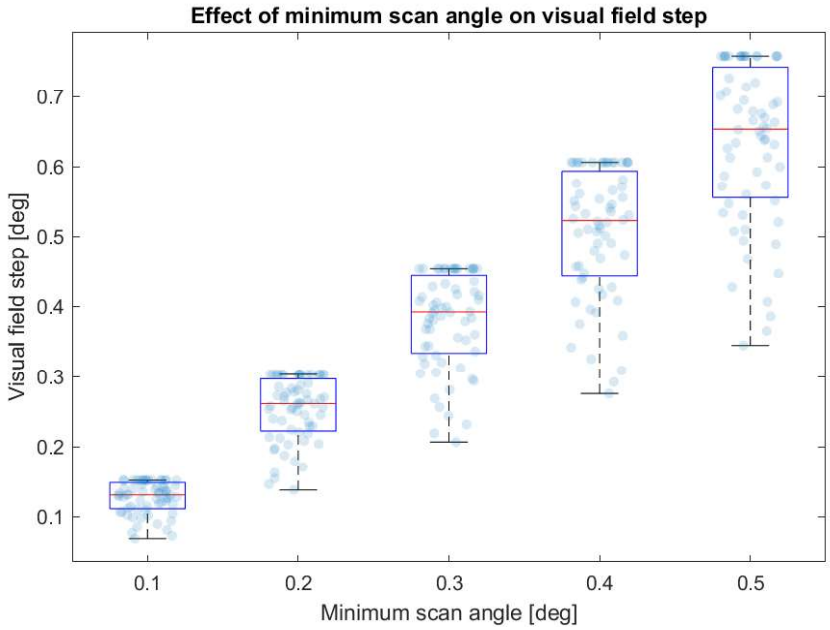

Figure 9. Effect of minimum scan angle of the galvo mirror on visual field step.

The smaller the minimum scan angle, the smaller the visual field step. This relation is clear since the step size of the galvo mirror angle should heavily influence the resultant visual field step size. The visual field step needs to be minimized to enable denser stimulation.

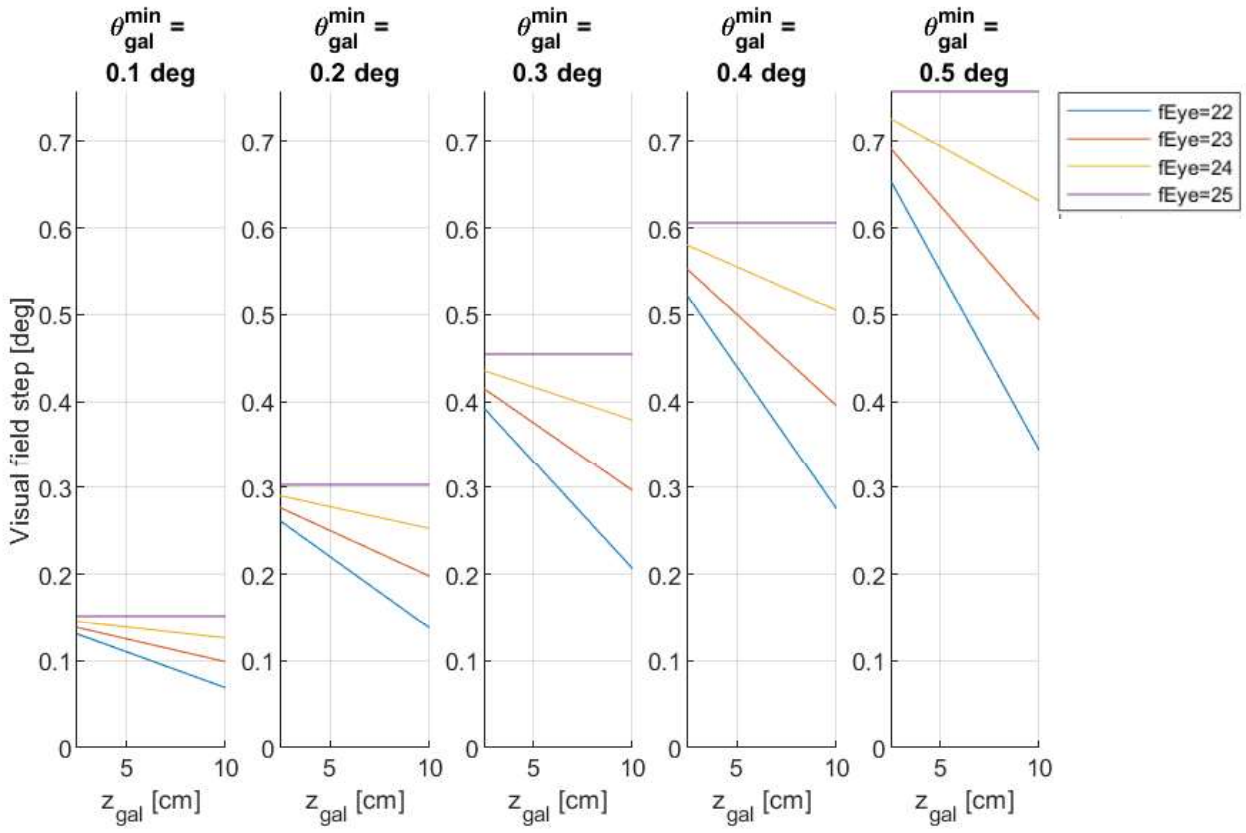

Figure 9. Resultant visual field step for all combinations of the three input parameters. As the maximum scan angle increases, the corresponding visual field step worsens.

Surprisingly, the visual field step size is minimized (i.e., the best) when the distance between the galvo mirror and eye is maximal. Thus, the system will exhibit a greater visual field, but enlarged or worse visual field step the closer the galvo mirror is to the eye. To optimize the system, the visual field should be maximized while the visual field step should be minimized. In this case, it is easier to consider an inverse visual field step as defined by the pixel number per degree. For a given maximum scan angle, minimum scan angle, pupil size and focal length,

visual field and pixel number ($\frac{1}{visual\ field\ step}$) can be plotted, clearly displaying the optimization tradeoff.

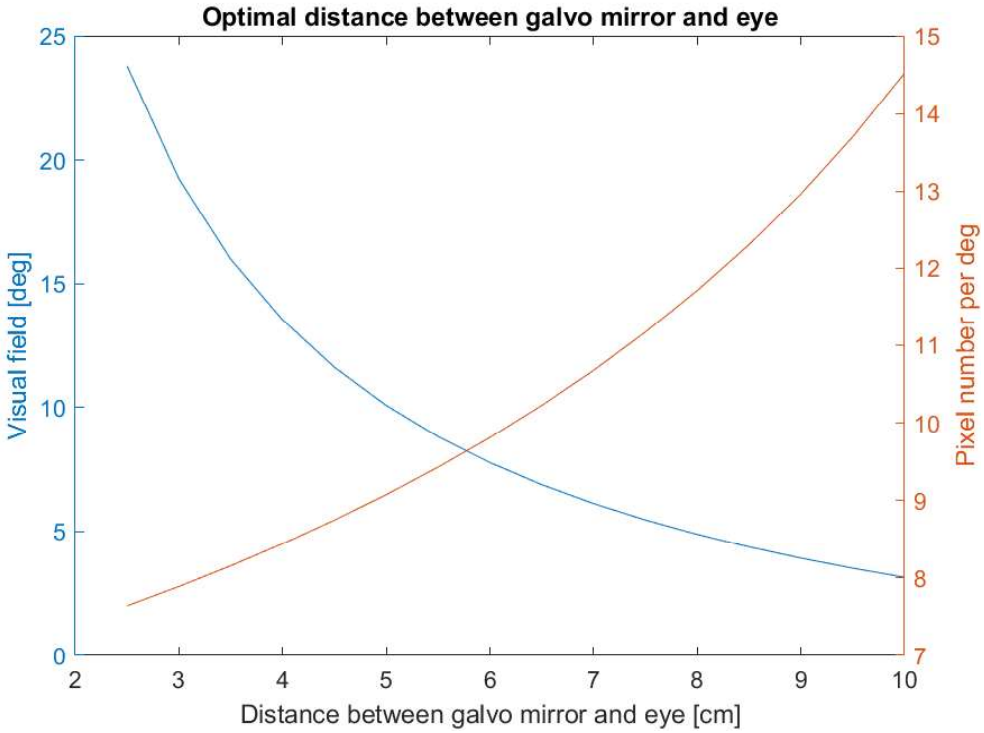

Figure 10. Visual field and visual field step given $a_{gal}^{max} = 20\ deg, a_{gal}^{min} = 0.1\ deg, d_{pupil} = 8\ mm, f_{eye} = 22\ mm$. The intersection of the two curves represents an optimal distance between the galvo mirror and eye.

It is interesting to note that the focal length of the eye heavily influences the visual field step (Fig. 9), despite not being controllable in this system. The visual field step is minimized when the focal length of the eye is shorter and the distance between the galvo mirror and the eye is large.

The visual field resolution of the system should not depend on the maximum scan angle, the minimum scan angle, or the distance between the galvo mirror and eye. A linear regression analysis of the visual field resolution determined that the primary only factors affecting visual field resolution are pupil size and the focal length of the eye. Thus, the theoretical resolution of the system is dictated by the uncontrollable human factors.

Table 4. Linear regression analysis of visual field resolution.

Variable	Coefficient	p-value
z_{gal}	-3.3083e-15	1
d_{beam}	-7.1484e-18	1
f_{eye}	0.53919	0
d_{pupil}	-2.9414	0
θ_{eff}^{max}	5.6484e-16	1
θ_{gal}^{min}	2.5015e-15	1

Surprisingly, the laser beam size did not affect the visual field resolution, perhaps because the unfocused cases dominated the focused, diffraction-limited cases and thereby the visual field resolution was mostly determined by the chief-peripheral ray divergence rather than the Airy disk spot size. An investigation of the standard deviation of the visual field resolution across maximum scan angle, minimum scan angle, distance between the galvo mirror and eye, and laser beam size confirms that these parameters negligibly influence visual field resolution.

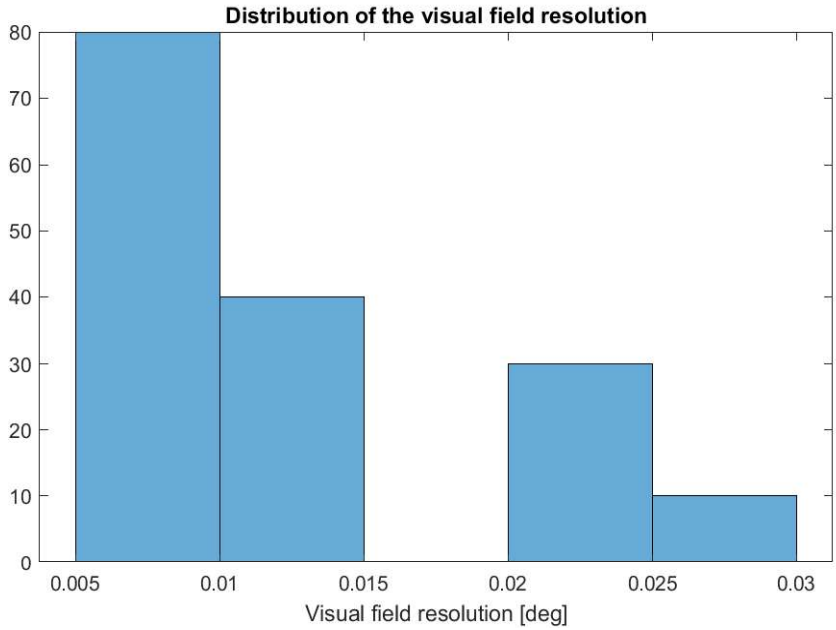

Figure 11. Histogram of the visual field resolution.

As a result, the visual field resolution of the system ranges between 0.006 and 0.03 degrees. The range corresponds to a laser beam spot size between 1.7 and 8.6 μm. In practice, a beam spot size of 1.7 μm will be difficult to achieve. In commercially available OCT systems, which have similar focusing optics and can be used for comparison, the probe beam spot size ranges between 10 and 30 μm.[20] Therefore, it is more reasonable to assume a beam spot in practice between 10 and 20 μm (0.03 and 0.06 deg in the visual angle) which is not limited by the design, which achieves a maximum spot size of 8.6 μm, but other factors like tissue scattering. Since the average retinal ganglion cells size is around 10 μm, the system could achieve near single-cell resolution, which should lead to improved clinical outcomes.

Discussion

There are several limitations to the simulation established in this paper. First, the system assumes the retina to be flat instead of curved for simplification. A curved retina affects where the laser beam rays fall onto the retina. Since visual field resolution depends on the divergence between the chief and peripheral rays, a curved surface introduces variation to the resolution. This is most evident in the peripheral retina, where the effect of the curvature of the retina is largest. A more robust system would properly account for the curvature of the system to calculate where the laser beam rays fall. Another assumption of the presented study was that the eye lens acts as a thin lens during the ray transfer matrix analysis. For a more anatomically correct model, the thickness of the eye lens is not negligible, and the eye lens should be considered as a thick lens. This can be done by replacing the thin lens RTM of the eye lens with an RTM of a thick lens which accounts for the curvature and thickness of the eye lens, as well as the refractive indices of the pupil and the eye. Lastly, for the RTM analysis, the laser beam was assumed to be a plane wave and thus the diffraction-limited focus spot size was calculated from an Airy disk. For more accurate calculations, the laser beam should be assumed as a Gaussian beam, where the diffraction-limited spot size is defined by the beam waist for the focused case. Assuming a Gaussian beam instead of a plane wave also changes the RTM analysis. For RTM analysis of a Gaussian beam, the complex beam parameter, which depends on the wavelength, radius of curvature and beam spot size, needs to be considered. Despite these margins to improve, we believe that the visual field, step, and resolution calculated here provide an important insight and design consideration when the benchtop system is instrumented.

The Argus II implant (SSMP) was the first electrode-based retinal implant to become commercially available and is still the only option currently available. It covers 11 to 19 degrees in the visual field (approximately 22 degrees diagonally) with a step size of 2 degrees. The best

visual acuity achieved by Argus II is 20/1,200, which gives a visual field resolution of 0.8 degrees.[9] This visual field would classify subjects as legally blind. A higher resolution state-of-the-art subretinal photovoltaic implant consisting of 1-2 mm sized arrays is currently being tested in animals for improved performance. Due to the small size of the arrays, they cover between 3.5 and 7 degrees of visual field, with a visual field step of 0.26 degrees and a visual field resolution of 0.35 degrees.[21] Thus, despite the high resolution, this photovoltaic implant offers a reduced visual field.

The visual field of the system proposed in this paper found to be up to 27.54 degrees, which encompasses roughly a fourth of normal vision. It is important to consider that while the restore visual field is marginal when compared to normal vision, retinal prosthetics aim to restore central vision, not all vision. In age-related macular degeneration, central vision is the first to degrade. Additionally, central vision is higher resolution than peripheral vision and we receive most of our visual information from central vision. Thus, a limited visual filed of around 20 to 30 degrees is still a viable outcome for its intended application. The upper limit of visual field is twice that of currently available systems and roughly five times that of high-resolution systems currently being developed. The visual field step outcome for the proposed system is distributed between 0.07 and 0.8 degrees, offering a much better step size than the commercially available human system (2 deg), and a comparable step size to the state-of-the-art animal-test system (0.26 deg). The visual field resolution of the system ranges between 0.006 and 0.03 degrees, which is better than both the human and the animal-test systems and achieves single-cell resolution. Thus, the proposed system offers improved visual field, step size, and resolution when compared to the existing systems.

For the analysis of this system, it was assumed that visual field should be maximized, and visual field step and resolution should be minimized. Thus, the optimal set up would exhibit a large visual field and a small visual field step. However, purely minimizing the visual field step with a maximal visual field could limit the scan speed of the system. The speed of the system, or frame rate, inversely depends on the number of pixels, which is in the order of $(\frac{visual\ field}{visual\ field\ step})^2$. Thus, if the visual field step is too small and the corresponding pixel number is large, the frames per second is reduced and the restored vision quality is reduced. There is a tradeoff between maximizing visual field and minimizing visual field step to achieve the desired frames per second. From the simulation of the system, it is evident that the distance between the galvo mirror and the lens heavily influences both the visual field and visual field step. As this is the parameter that can be modulated most easily, optimizing this value to maximize the visual field and minimize visual field step while maintaining an appropriate frame rate, will optimize the performance of the system.

Another important takeaway based on the simulation of the system is that the maximum scan angle is primarily limited by pupil size in most cases. This reveals that the maximum scan angle of the galvo mirror does not need to be that large as a maximum scan angle of 20 degrees gives desirable results. In general, galvo mirrors with larger maximum scan angles are more expensive. The fact that the maximum scan angle in the system is limited by pupil size means that a more affordable galvo mirror with a range of around 20 degrees can be utilized. A suitable selection for this system would be a galvo mirror with a scan angle of 25 degrees, such as the Compact 506 (ScannerMax).

Conclusion

Electrode-based retinal prosthesis implants have shown favorable results in restoring vision in subjects with vision loss. However, due to limitations of these implants, there is a need for a contact-free and damage-free solution for vision restoration. AuNR-enhanced NIR stimulation of retinal ganglion cells offers a spatially selective, artifact-free method of restoring vision that does not damage the tissue. The simulation performed in this study uses ray transfer matrix analysis to trace the laser beam rays through the system to provide insight into important design considerations for a bench-top retinal prosthesis system that uses AuNR-enhanced NIR stimulation. From an initial investigation, the specifications of the galvo mirror, particularly the maximum scan angle, and the laser beam diameter appear to be the driving factors in determining the visual field output. However, the results presented in this study suggest that due to limitations set by the size of the pupil, the maximum scan angle does not heavily factor into the results. The system requires a galvo mirror scan angle of around 20 degrees, which is easily achieved by an affordable galvo mirror set, such as the Compact 506 suggested in this paper.

Additionally, the effect of the initial laser beam diameter was found to be negligible within the tested range, as the visual field resolution was mostly determined by the chief-peripheral ray divergence in unfocused cases, rather than the Airy disk spot size in focused cases. Pupil diameter of the subject and focal length were found to heavily influence the resultant visual field, step size, and resolution, but are uncontrollable human factors that vary subject to subject. Despite being uncontrollable, it is important to investigate how these factors affect performance as in its application, a AuNR-enhanced NIR stimulation based retinal prosthesis will have to account for the changes in these factors to offer the best performance. The simulation also revealed that the distance between the galvo mirror and the eye surface is a key parameter to modulate in order to optimize visual field and visual field step. From the results of the

simulation, it is evident that the proposed system achieves favorable visual field, step size, and resolution when compared to commercially available and experimental electrode-based retinal prostheses. AuNR-enhanced NIR stimulation is a feasible method for non-invasive retinal prosthesis.

References

[1] Pascolini, Donatella, and Silvio Paolo Mariotti. “Global Estimates of Visual Impairment: 2010.” British Journal of Ophthalmology 96, no. 5 (January 2011): 614–18. https://doi.org/10.1136/bjophthalmol-2011-300539.

[2] Margalit, Eyal, Mauricio Maia, James D Weiland, Robert J Greenberg, Gildo Y Fujii, Gustavo Torres, Duke V Piyathaisere, et al. “Retinal Prosthesis for the Blind.” Survey of Ophthalmology 47, no. 4 (2002): 335–56. https://doi.org/10.1016/s0039-6257(02)00311-9.

[3] Lefevere, Evy, Anne Katrine Toft-Kehler, Rupali Vohra, Miriam Kolko, Lieve Moons, and Inge Van Hove. “Mitochondrial Dysfunction Underlying Outer Retinal Diseases.” Mitochondrion 36 (2017): 66–76. https://doi.org/10.1016/j.mito.2017.03.006.

[4] Lim, LS, P Mitchell, JM Seddon, FG Holz, and TY Wong. “Age-Related Macular Degeneration.” Lancet, May 5, 2012, 1728–38. https://doi.org/10.1016/S0140-6736(12)60282-7.

[5] Margalit, Eyal, and Srinivas R. Sadda. “Retinal and Optic Nerve Diseases.” Artificial Organs 27, no. 11 (2003): 963–74. https://doi.org/10.1046/j.1525-1594.2003.07304.x.

[6] Wells, Jonathon, Chris Kao, Karthik Mariappan, Jeffrey Albea, E. Duco Jansen, Peter Konrad, and Anita Mahadevan-Jansen. “Optical Stimulation of Neural Tissue in Vivo.” Optics Letters 30, no. 5 (January 2005): 504. https://doi.org/10.1364/ol.30.000504.

[7] Polikov, Vadim S., Patrick A. Tresco, and William M. Reichert. “Response of Brain Tissue to Chronically Implanted Neural Electrodes.” Journal of Neuroscience Methods 148, no. 1 (2005): 1–18. https://doi.org/10.1016/j.jneumeth.2005.08.015.

[8] Behrend, Matthew R., Ashish K. Ahuja, Mark S. Humayun, Robert H. Chow, and James D. Weiland. “Resolution of the Epiretinal Prosthesis Is Not Limited by Electrode Size.” IEEE Transactions on Neural Systems and Rehabilitation Engineering 19, no. 4 (2011): 436–42. https://doi.org/10.1109/tnsre.2011.2140132.

[9] Stronks, H Christiaan, and Gislin Dagnelie. “The Functional Performance of the Argus II Retinal Prosthesis.” Expert Review of Medical Devices 11, no. 1 (2013): 23–30. https://doi.org/10.1586/17434440.2014.862494.

[10] Walker, H. Kenneth., W. Dallas. Hall, and J. Willis. Hurst. “Chapter 116. Visual Fields.” In Clinical Methods: the History, Physical and Laboratory Examinations. Boston: Butterworths, 1990.

[11] Farnum, Alexander, and Galit Pelled. “New Vision for Visual Prostheses.” Frontiers in Neuroscience 14 (2020). https://doi.org/10.3389/fnins.2020.00036.

[12] Shapiro, Mikhail G., Kazuaki Homma, Sebastian Villarreal, Claus-Peter Richter, and Francisco Bezanilla. “Infrared Light Excites Cells by Changing Their Electrical Capacitance.” Nature Communications 3, no. 1 (2012). https://doi.org/10.1038/ncomms1742.

[13] Albert, E. S., J. M. Bec, G. Desmadryl, K. Chekroud, C. Travo, S. Gaboyard, F. Bardin, et al. “TRPV4 Channels Mediate the Infrared Laser-Evoked Response in Sensory Neurons.” Journal of Neurophysiology 107, no. 12 (2012): 3227–34. https://doi.org/10.1152/jn.00424.2011.

[14] Wells, Jonathon D., Sharon Thomsen, Peter Whitaker, E. Duco Jansen, Chris C. Kao, Peter E. Konrad, and Anita Mahadevan-Jansen. “Optically Mediated Nerve Stimulation: Identification of Injury Thresholds.” Lasers in Surgery and Medicine 39, no. 6 (2007): 513–26. https://doi.org/10.1002/lsm.20522.

[15] Yong, Jiawey, Karina Needham, William G. A. Brown, Bryony A. Nayagam, Sally L. Mcarthur, Aimin Yu, and Paul R. Stoddart. “Gold-Nanorod-Assisted Near-Infrared Stimulation of Primary Auditory Neurons.” Advanced Healthcare Materials 3, no. 11 (May 2014): 1862–68. https://doi.org/10.1002/adhm.201400027.

[16] Qing, Ruobing, Oscar M. Carrasco-Zevallos, Shwetha Mangalesh, Neeru Sarin, Lejla Vajzovic, Sina Farsiu, Joseph A. Izatt, and Cynthia A. Toth. “Characterization of Long Working Distance Optical Coherence Tomography for Imaging of Pediatric Retinal Pathology.” Translational Vision Science and Technology, October 16, 2017. https://doi.org/10.1167/tvst.6.5.12.

[17] Walker, H. Kenneth., W. Dallas. Hall, and J. Willis. Hurst. “Chapter 58. The Pupils.” In Clinical Methods: the History, Physical and Laboratory Examinations. Boston: Butterworths, 1990.

[18] Perkins, Edward S., and Hugh Davson. “Human Eye.” Encyclopædia Britannica. Encyclopædia Britannica, inc., June 22, 2018. https://www.britannica.com/science/human-eye.

[19] Drasdo, N, and C W Fowler. “Non-Linear Projection of the Retinal Image in a Wide-Angle Schematic Eye.” British Journal of Ophthalmology 58, no. 8 (January 1974): 709–14. https://doi.org/10.1136/bjo.58.8.709.

[20] Braaf, Boy, Kari V. Vienola, Christy K. Sheehy, Qiang Yang, Koenraad A. Vermeer, Pavan Tiruveedhula, David W. Arathorn, Austin Roorda, and Johannes F. De Boer. “Real-Time Eye Motion Correction in Phase-Resolved OCT Angiography with Tracking SLO.” Biomedical Optics Express 4, no. 1 (November 2012): 51. https://doi.org/10.1364/boe.4.000051.

[21] Lorach, Henri, Georges Goetz, Richard Smith, Xin Lei, Yossi Mandel, Theodore Kamins, Keith Mathieson, et al. “Photovoltaic Restoration of Sight with High Visual Acuity.” Nature Medicine 21, no. 5 (2015): 476–82. https://doi.org/10.1038/nm.3851.